Revealing Eu^{3+}-doped Yttrium pyrogermanate as soft UV excitable phosphor: Retains Pros of commercial phosphor and compensates for Cons

Adish Tyagi[1,2], Sandeep Nigam*[1,2], B. G. Vats[3], V. Sudarsan[1,2], C. Majumder[1,2], R. Kaiwart[4], H. K. Poswal[4], Jagannath[5], A. K. Tyagi[1,2]

[1]Chemistry Division, Bhabha Atomic Research Center, Mumbai, 400 085 INDIA.

[2]Homi Bhabha National Institute (HBNI), Mumbai, 400 094, INDIA

[3]Fuel Chemistry Division, Bhabha Atomic Research Center, Mumbai, 400 085 INDIA

[4]High Pressure and Synchrotron Radiation Physics Division, Bhabha Atomic Research Center, Mumbai, 400 085 INDIA

[5]Technical Physics Division, Bhabha Atomic Research Center, Mumbai, 400 085 INDIA.

Supporting Information

Experimental and computational detail:

(a)

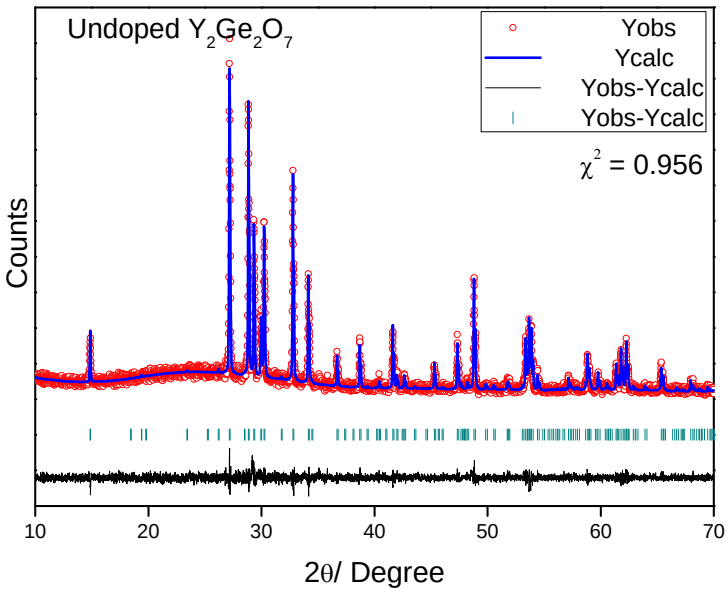
Undoped $Y_2Ge_2O_7$
Yobs
Ycalc
Yobs-Ycalc
Yobs-Ycalc
χ^2 = 0.956
Counts
10
20
30
40
50
60
70
2θ/ Degree

(b)

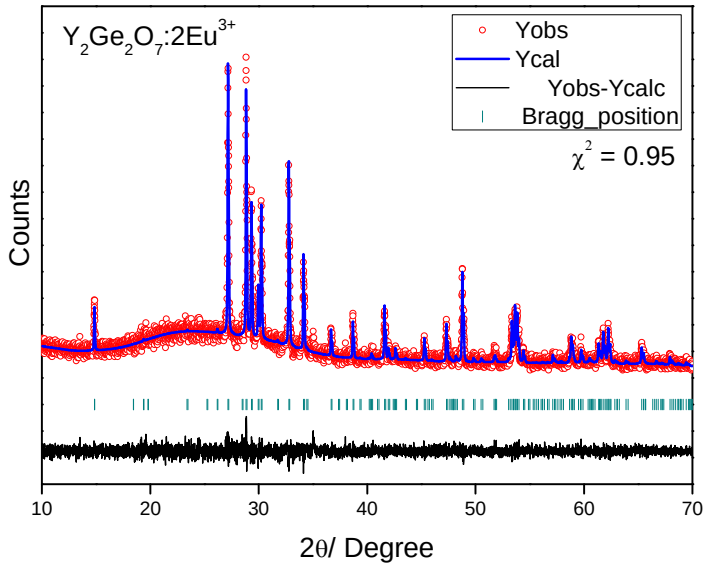
$Y_2Ge_2O_7$:2Eu^{3+}
Yobs
Ycal
Yobs-Ycalc
Bragg_position
χ^2 = 0.95
Counts
10
20
30
40
50
60
70
2θ/ Degree

(c)

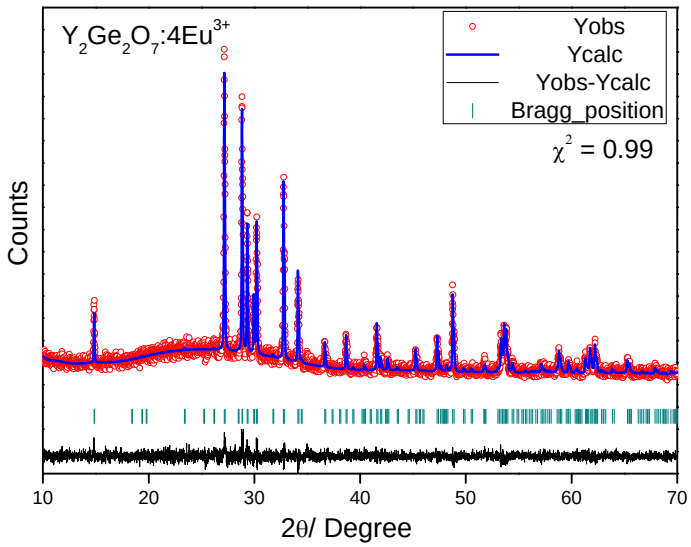
$Y_2Ge_2O_7$:4Eu^{3+}
Yobs
Ycalc
Yobs-Ycalc
Bragg_position
χ^2 = 0.99
Counts
10
20
30
40
50
60
70
2θ/ Degree

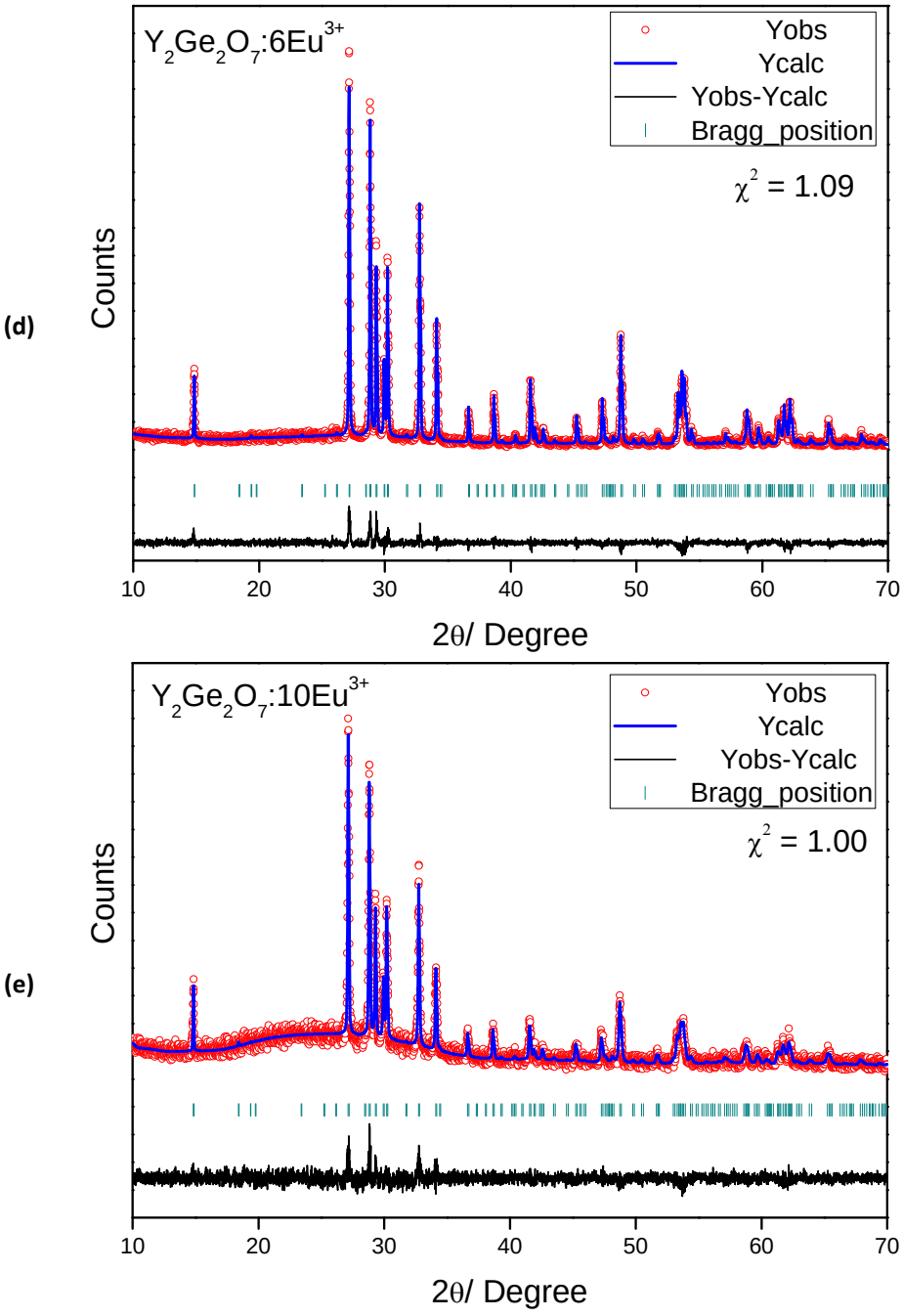

Figure-S1: XRD Pattern and respective Rietveld Refinement of $Y_2Ge_2O_7$: Eu samples with varying Eu concentration

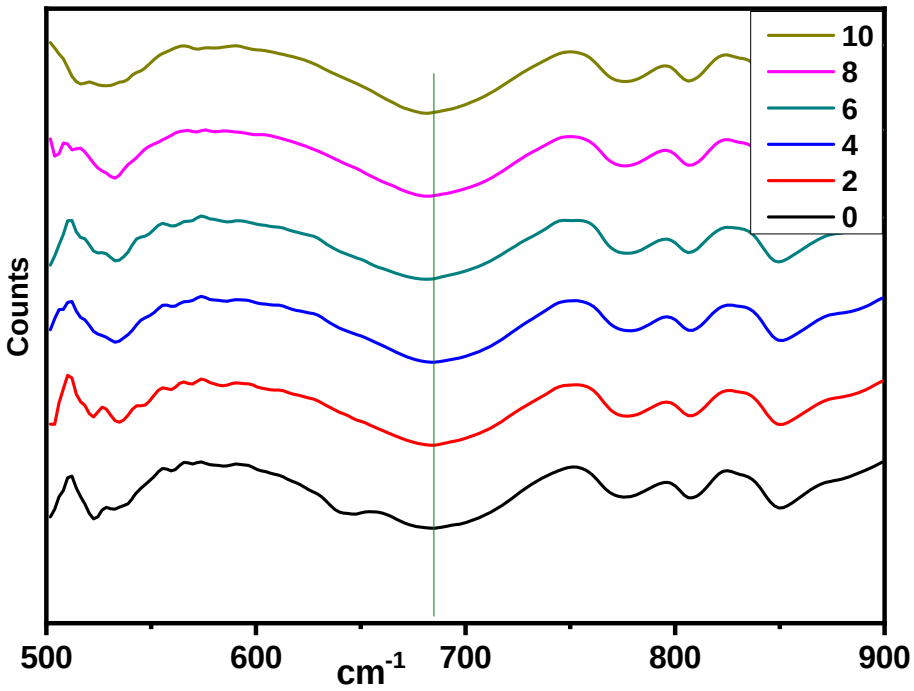

Figure-S2:FTIR spectrum of undoped and Eu-doped $Y_2Ge_2O_7$.

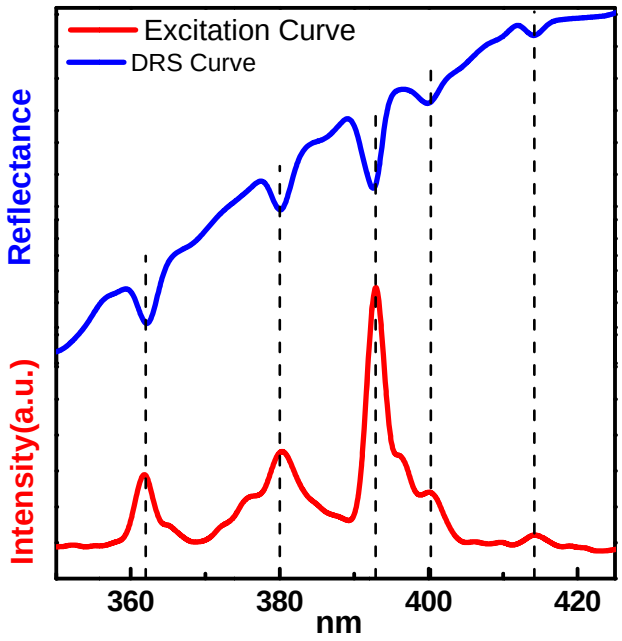

Figure-S3: Coherence of Diffuse Reflectance spectra (DRS) and excitation spectra of $Y_2Ge_2O_7$:Eu.

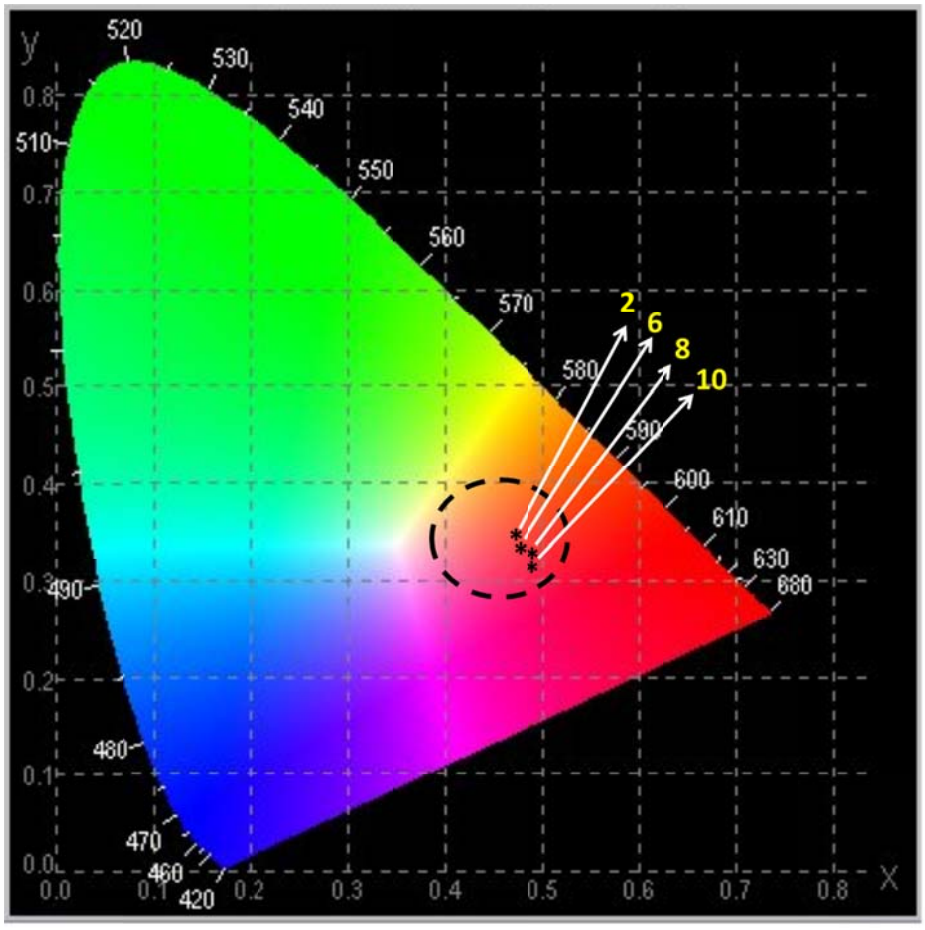

Figure-S4: CIE Chromaticity Diagram of $Y_2Ge_2O_7$: Eu phosphor with different Eu-content.

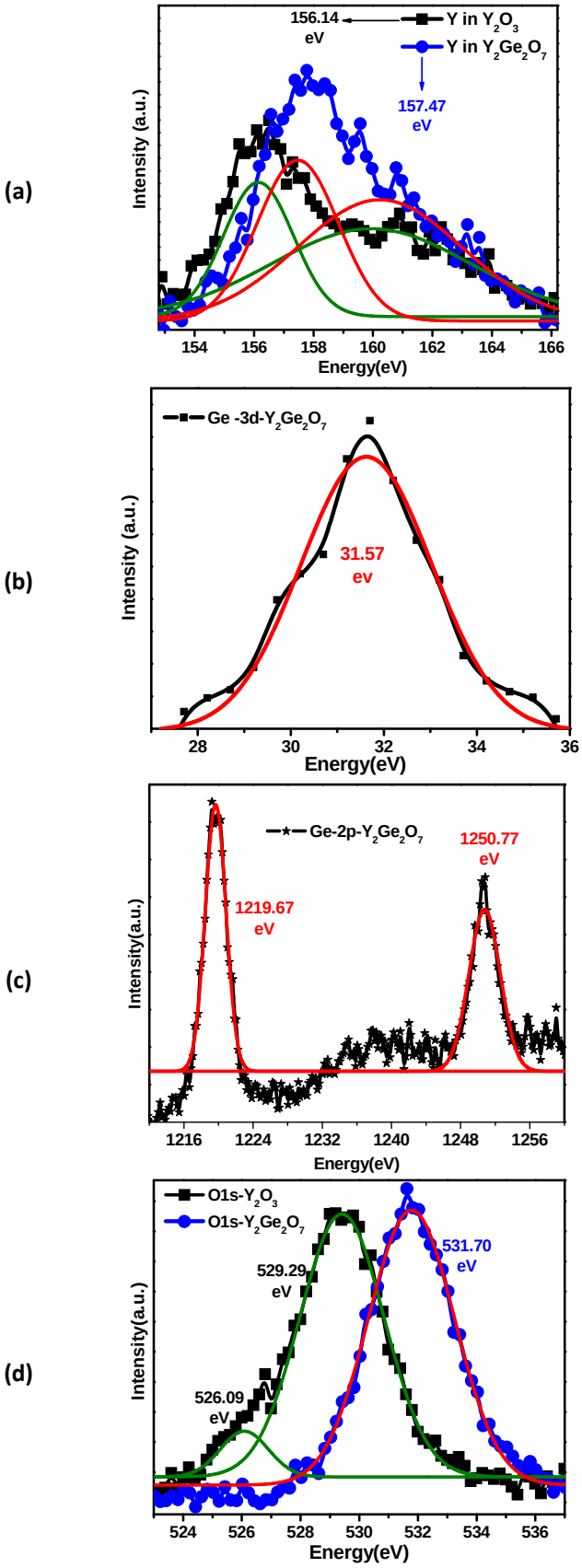

Figure-S5: XPS of Y_2O_3:Eu and$Y_2Ge_2O_7$:Eu samples (2%Eu).

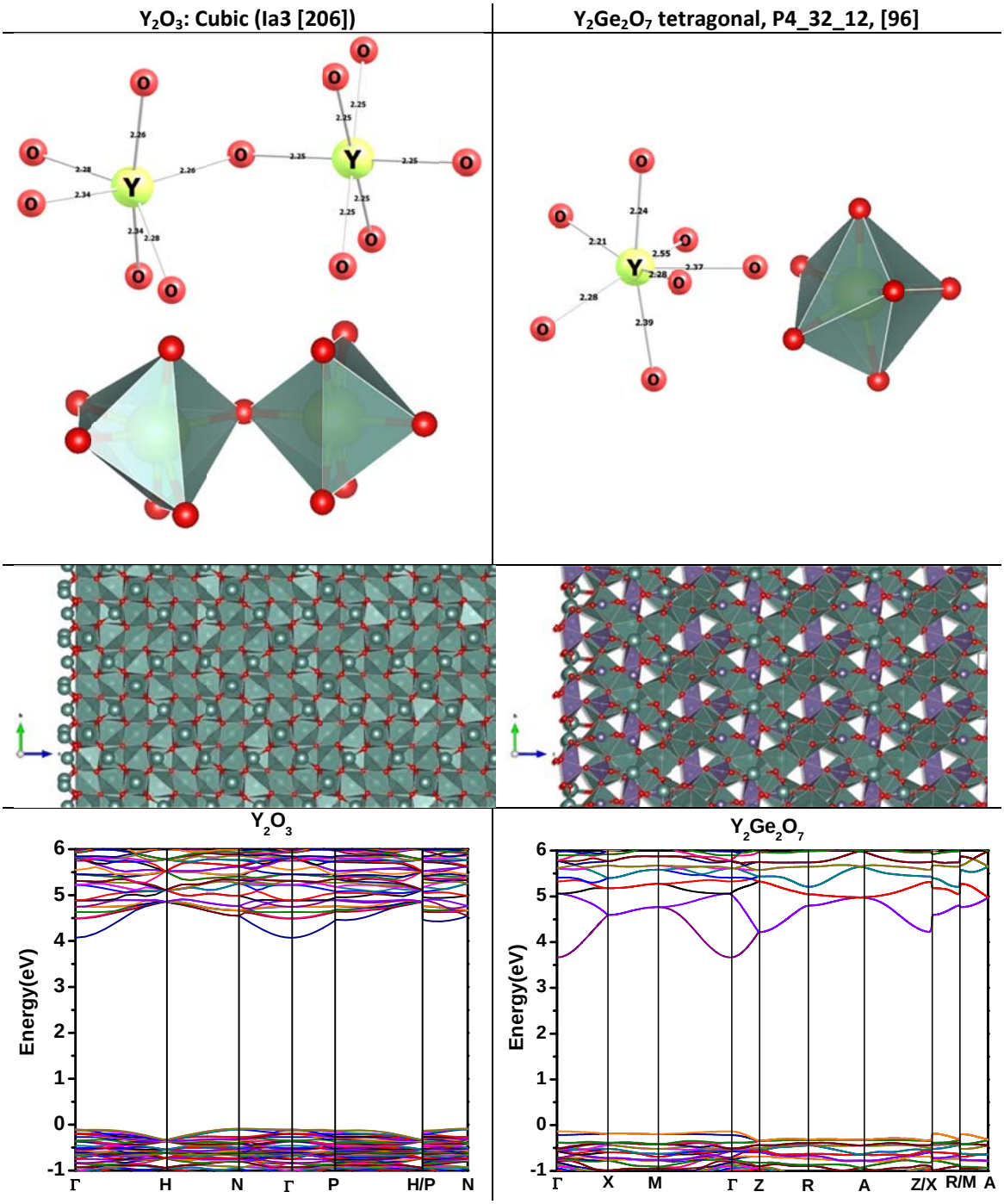

Figure-S6: Comparison of geometry and electronic structure of Y_2O_3 and $Y_2Ge_2O_7$.

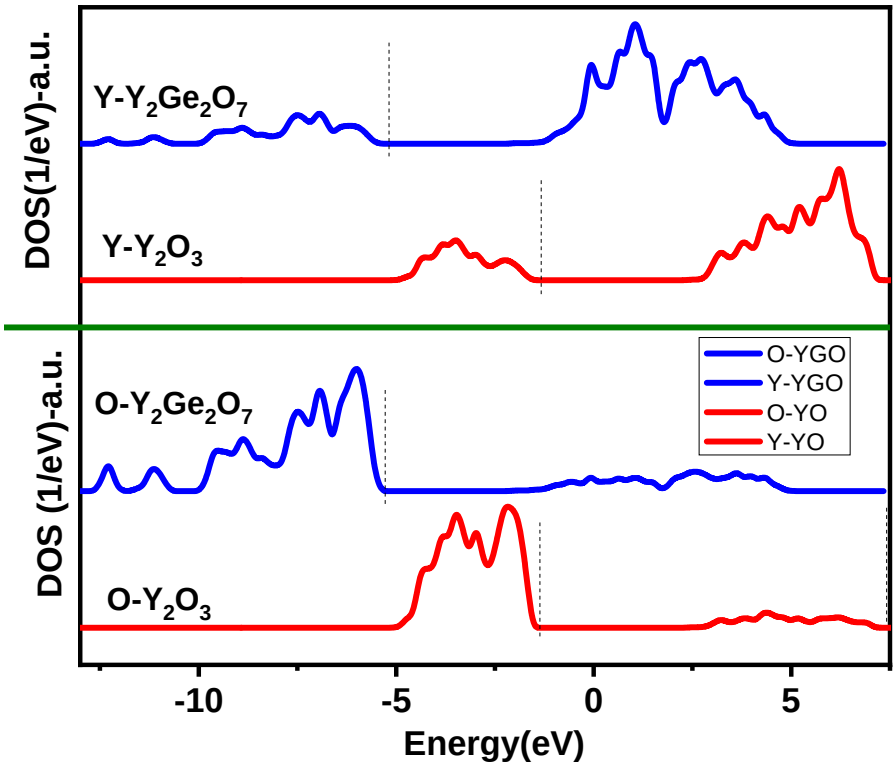

Figure-S7: *Comparison of projected density of states of Y_2O_3 and $Y_2Ge_2O_7$. The vertical line indicates the Fermi level*

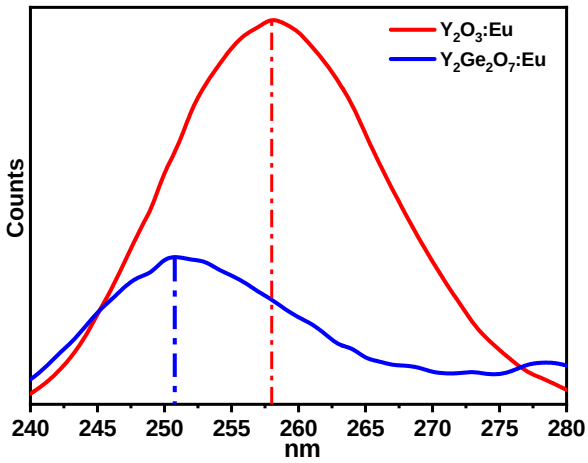

Figure-S8: Comparison of charge transfer band of $Y_2Ge_2O_7$:Eu and Y_2O_3:Eu phosphor.

1. Experimental and computational details section

Materials and methods

GeO_2, Y_2O_3 and Eu_2O_3 were obtained from Analytical Reagent grade, SD Fine Chemicals, Mumbai, India and were used as received. Powder XRD date of the samples was recorded using Cu Kα (λ = 1.5405 Å) using monochromatic X-ray source of a Rigaku Miniflex-600 diffractometer. The pattern of the samples was recorded in the range of 10-70° (2θ) in continuous mode. Fourier transformed infrared (FTIR) spectra were recorded with a resolution of 2 cm^{-1} for thin pellets of the samples made in KBr matrix on a Bomem MB102 FTIR spectrometer. All the luminescence measurements were carried out at room temperature on an Edinburgh Instruments' FLSP 920 system, having a 450W Xe lamp and a micro-second flash lamp (60W) as excitation sources. Red sensitive PMT was used as the detector. Approximately 20mg of compound was mixed with few drops of methanol and the resulting slurry was spread over a glass plate. This was dried under ambient conditions and used for luminescence measurements. All emission spectra were corrected for detector response and excitation spectra for the lamp profile. Raman scattering experiment have been performed on Jobin Yvon triple-stage T64000 Raman spectrometer in a back-scattering geometry coupled with charge couple device (CCD) detector in single mode configuration. For Raman signal excitation, He-Ne laser of wavelength 632.8 are used. Raman modes have been collected with 20x object lens, which are dispersed by grating of density 1800 grooves/mm in the range of 100-1000 cm^{-1}. The resolution of the system with this configuration is < 4 cm^{-1}.XPES analysis on the samples were performed at 4064 eV photon energy on thePES-BL14 beamline (BARC) at Indus-2, RRCAT, Indore.

Synthesis

$Y_{2-x}Ge_2O_7:xEu^{3+}$ (x = 0, 0.02,0.04, 0.06, 0.08, 0.10, 0.15, 0.20) samples were prepared through high temperature solid state route. For this stoichiometric amount of Y_2O_3 (Merck, 99.99%) GeO_2 Merck, ≥ 99.99%)and Eu_2O_3 (Merck, 99.9%) were well mixed and then heated at 1300 °C for 8 hours in air. After cooling to the ambient temperature, all the samples were ground into powder for further measurements.

Computational Details:

All calculations were carried out using the spin-polarized DFT with a plane wave basis set, implemented in the Vienna Ab-initio Simulation Package (VASP)[1-2]. The electron–ion interactions were described by the projector augmented wave (PAW) method[3]. PAW pseudo potentials generated using with scalar relativistic corrections are used[4]. The spin polarized generalized gradient approximation using the Perdew–Burke–Ernzerhof (PBE) functional[5] has been used to calculate the exchange-correlation energy. The cut off energy for the plane wave basis set was fixed at 400 eV for

all calculations performed in this study. The geometry optimization was performed by ionic relaxation, using a conjugate gradient minimization. The geometries are considered to be converged when the force on each ion becomes 0.01eV/ Å or less. The total energy convergence was tested with respect to the plane-wave basis set size and simulation cell size, and the total energy was found to be accurate to within 1 meV. A Monkhorst-Pack k-point grid of 6 x 6 x 6 was employed to map the first Brillouin zone.

Three-dimensional periodic boundary conditions were applied to approximate a bulk solid. Conventional tetragonal unit cell containing 44 atoms (8 Y, 8 Ge, 28 O) were used for calculations. Structural optimization was performed with respect to atomic coordinates and unit-cell parameters. The calculated lattice parameter (*a*=*b*=6.883 Å *c*=12.348 Å; α=β=γ=90^o) and structural parameter are in excellent agreement with the reported experimental values[6]. The simulated XRD pattern of DFT structure of $Y_2Ge_2O_7$ also matches very well with experimental counterpart. The calculation for Y_2O_3 was carried out using unit cell having 64 atoms (32Y, 48O). The calculated lattice parameters (a=10.614 Å; α=β= γ=90^o). The for Eu-doping in $Y_2Ge_2O_7$ and Y_2O_3, one yttrium atom from the unit cell was replaced with europium. The total magnetic moment of the unit cell was found to be six belonging to $4f^6$ configuration of Eu^{3+}.

Ω_λ, where λ = 2 and 4Parameter and quantum efficiency calculation:

In the present study, Ω_λ values have been calculated by considering the $^5D_0 \rightarrow {}^7F_1$ transition as the reference[7]. Emission intensity can be expressed by the relation I = N ħ ω A, where, N is the population of the emitting level ($^5D_0$), ħ ω is the transition energy and A is the Einstein's coefficient of spontaneous emission.[8,9] The terms "A" and Ω_λ are related through the following expression (equation 1)

$$A_{0\text{-}\lambda} = \frac{64\pi^4 \nu^3 e^2}{3hc^3} \frac{1}{4\pi\varepsilon_0} \chi \sum_\lambda \Omega_\lambda \left\langle {}^5D_0 \left\| U^\lambda \right\| {}^7F_J \right\rangle^2 \quad \ldots(1)$$

Where "ν" is the frequency, "h" is the Plank's constant, "e" is the charge of the electron, "$1/4\pi\varepsilon_0$" is a constant and is equal to 8.99 x 10^9 Nm^2/C^2, "χ" is Lorents field correction and is equal to $n_0(n_0^2+2)^2/9$, where n_0 is the refractive index of the material. The value of refractive index is taken as 1.78 and is obtained by taking the average value of the refractive indices corresponding to GeO_2 and Y_2O_3 phases.[19] The term $\left\langle {}^5D_0 \left\| U^\lambda \right\| {}^7F_J \right\rangle^2$ is the square of the reduced matrix elements. The values of $\left\langle {}^5D_0 \left\| U^2 \right\| {}^7F_2 \right\rangle^2$ and $\left\langle {}^5D_0 \left\| U^4 \right\| {}^7F_4 \right\rangle^2$ are taken as 0.0032 and 0.0023, respectively[10]. The values of the spontaneous emission cross-section is calculated from the emission spectrum using the relation $A_{0\text{-}\lambda} = (\nu_{0\text{-}1}/\nu_{0\text{-}\lambda})(I_{0\text{-}\lambda}/I_{0\text{-}1})A_{0\text{-}1}$,[8,11] where $\nu_{0\text{-}\lambda}$ and $I_{0\text{-}\lambda}$ represent respectively the frequency and intensity corresponding to the respective transition in the emission spectrum. $A_{0\text{-}1}$ is taken as a constant[10] and

is equal to 50 s^{-1}. As the matrix elements $U^{(4)}$, $U^{(6)}$ and $U^{(2)}$, $U^{(6)}$for the $^5D_0 \rightarrow {}^7F_2$ and $^5D_0 \rightarrow {}^7F_4$transitions,respectively are very small (negligible), the values of Ω_2 and Ω_4 can be calculated from equation 1 bydetermining $A_{0-\lambda}$directly from the emission spectrum.

The quantum efficiency values are calculated by taking the ratio of radiative decay rates and total (radiative + non-radiative) decay rates. Emission quantum efficiency [$\eta = A_{rad}/(A_{rad}+A_{nrad})$].

The radiative decay rate (A_{rad}) is calculated by summing of all the spontaneous emission cross-section ($A_{0-\lambda}$) values, λ= 0,1,2,3,4. For example A_{0-2} and A_{0-4} corresponds to spontaneous emission cross-section for the $^5D_0 \rightarrow {}^7F_2$ and $^5D_0 \rightarrow {}^7F_4$ transitions. The values of the spontaneous emission cross-section is calculated from the emission spectrum using the relation $A_{0-\lambda} = (\nu_{0-1}/\nu_{0-\lambda})(I_{0-\lambda}/I_{0-1})A_{0-1}$, where $\nu_{0-\lambda}$ and $I_{0-\lambda}$ represent respectively the frequency and intensity corresponding to the respective transition in the emission spectrum. A_{0-1} is taken as a constant value of $50s^{-1}$. Inverse of the experimentally measured lifetime ($1/\tau_{measured}$) gives the sum of non-radiative and radiative decay rates ($A_{rad} + A_{nrad}$).

Change is asymmetry Ratio:

In the undoped sample each Y^{3+} is having 7 oxygen atoms as near neighbours and $5Y^{3+}$ and $6Ge^{4+}$ as next nearest neighbours (NNN). With increasing Eu^{3+} doping, Y^{3+} ions existing as next nearest neighbors around a central (focal) Eu^{3+} will be replaced with another Eu^{3+} species. As a result, there will be six possible different configurations/structural units(*Eu^{3+} distribution and surrounding arrangements in the lattice*) with (n) Y^{3+} ions and (5-n) Eu^{3+} ions as next nearest neighbours. All these six configurations also have $6Ge^{4+}$ as next nearest neighbours. The relative concentrations of each of the six possible structural units existing in the solid solution with formula $(Y_{1-x}Eu_x)_2Ge_2O_7$ can be evaluated, assuming a binomial distribution based on Equation 2 as given below[12-14].

$$^{5-n}P_n = 5C_n[x]^n[1-x]^{5-n} \quad \text{.....(Eqn. 1).}$$

where "x" is the fraction of Eu^{3+} species in the solid solution (sample) and $^{5-n}P_n$ represents probability of Eu^{3+} structural units having "n" number of Y^{3+} and 5-n number of Eu^{3+} as next nearest neighbours. The term ^5C_n is given by the following equation (Equation 2).

$$5C_n = \frac{5!}{(5-n)!\times n!} \quad \text{.....(Eqn. 2)}$$

The calculated values of relative concentrations of different Eu^{3+} structural units are given in Table S1. It may be noted that structural units with concentration more than 0.2% are only mentioned in Table S1. As expected with increase in Eu^{3+} concentration, relative concentration of Eu^{3+} structural units with higher number of Eu^{3+} as next nearest neighbours increases (Table 1 of main manuscript).

For the samples investigated in the present study, mainly Eu^{3+} structural units with x=0, 1, 2, 3, 4, and 5 Eu^{3+} along with $6Ge^{4+}$ as next nearest neighbours, represented as Eu(5Y,0Eu, 6Ge), Eu(4Y,1Eu, 6Ge), Eu(3Y,2Eu, 6Ge), Eu(2Y,3Eu, 6Ge), Eu(1Y,4Eu, 6Ge) and Eu(0Y,5Eu, 6Ge) with varying concentrations are present as can be seen from Table S1. The main Eu^{3+} configurations existing in Eu^{3+} doped samples are primarily Eu(5Y,0Eu, 6Ge), Eu(4Y,1Eu, 6Ge), Eu(3Y,2Eu, 6Ge), and variation in the relative concentration is responsible for the variation in the values of asymmetric ratios

Table-S1: Cell parameters obtained via Rietveld Refinement

samples	a	b	c
Undoped $Y_2Ge_2O_7$	6.80150	6.80150	12.36905
$Y_2Ge_2O_7$:2Eu	6.80323	6.80323	12.37340
$Y_2Ge_2O_7$:4Eu	6.80480	6.80480	12.37632
$Y_2Ge_2O_7$:6Eu	6.80691	6.80691	12.38016
$Y_2Ge_2O_7$:8Eu	6.80802	6.80802	12.38212
$Y_2Ge_2O_7$:10Eu	6.80984	6.80984	12.38632

Table S2. Relative percentages of different Eu^{3+} structural units with varying number of $Y^{3+}$and Eu^{3+}as next nearest neighbours around a central (focal) Eu^{3+} ions in $Y_2Ge_2O_7$ lattice. Structural units with concentrations

Composition	Eu (5Y,0Eu, 6Ge) (%)	Eu (4Y,1Eu, 6Ge) (%)	Eu (3Y,2Eu, 6Ge) (%)	Eu (2Y,3Eu, 6Ge) (%)	Eu (1Y,4Eu, 6Ge) (%)	Eu (0Y,5Eu, 6Ge) (%)
x = 0.00	100	0	0	-	-	-
x = 0.02	90.4	9.2	0.4	-	-	-
x= 0.04	81.6	17.0	1.4	-	-	-
x = 0.06	73.4	23.4	3.0	0.20	-	-
x = 0.08	65.9	28.7	5.0	0.40	-	-
x = 0.10	59.0	32.8	7.3	0.9	-	-

REFERENCES (*cited in supporting information document*)

(1). Kresse, G.;Furthmuller, J. Efficient iterative schemes for ab initio total-energy calculations using a plane-wave basis set.*Phys. Rev. B*. 1996, 54, 11169-86.

(2). Vanderbilt, D.; Soft self-consistent pseudopotentials in generalized eigenvalue formalism *Phys. Rev. B.* 1990, 41, 7892-95.

(3). Blochl, P. E.; Projector augmented-wave method *Phys. Rev. B.* 1994, 50, 17953-79.

(4). Kresse, G.;Joubert, J. From ultrasoftpseudopotentials to the projector augmented-wave method, *Phys. Rev. B*. 1999, 59, 1758-75

(5). Perdew, J. P.;Chevary, J. A.;Vosko, S. K.; Jackson, K. A.; Pederson, M. R.; Singh, D. J.;Fiolhias, C. Atoms, molecules, solids, and surfaces: Applications of the generalized gradient approximation for exchange and correlation *Phys. Rev. B.* 1992; 46: 6671-87

(6). Redhammer, G.J.; Roth, G.; Amthauer, G. 'Yttrium pyrogermanate, $Y_2Ge_2O_7$*ActaCryst.* 2007, C63, i93-i95.

(7). C.A. Kodaira, H.F. Brito, O. L. Malta and O. A. Serra, *J. Lumin.* 2003, **101,** 11.

(8). D. Hreniak, W. Strek, J. Amami, Y. Guyot, G. Boulon, C. Goutaudier and R. Pazik, *J. Alloys. Compd.,* 2004, **380,** 348.

(9). L. M. Dennis and A. W. Laubengayer, *J. Phys. Chem.,* 1926, **30,** 1510.
(10). P. Dorenbos, in: W. M. Yen, S. Shionoya, H. Yamamoto (Eds.), *Phosphor hand book,*CRC press, Boca Raton, 2007, 142.
(11). W. T. Carnall, H. Crosswhite, H. M. Crosswhite, *Energy Structure and Transition Probabilities of the Trivalent Lanthanides in LaF_3,* Argonne National Laboratory Report, USA, 1977
(12). S.K. Kulshreshtha, R. Sasikala, V. Sudarsan, Non-random distribution of cations in $Sn_{1-x}Ti_xO2$ ($0.0 \leq \times \leq 1.0$): A ^{119}Sn MAS NMR study, *J. Mater. Chem.* **11** (2001) 930–935.
(13). S.K. Kulshreshtha, O.D. Jayakumar, V. Sudarsan, Non-random cation distribution in hexagonal $Al_{0.5}Ga_{0.5}PO_4$, *J. Solid State Chem.***183** (2010) 1071–1074.
(14). Dinesh K. Patel, K. G. Girija, Boddu S. Naidu, B. Vishwanadh, Farheen N. Sayed, R.K. Vatsa, V. Sudarsan, S. K. Kulshreshtha, *J. Alloys Compd.***884** (2021)161021 1-10